Article

Application of Active Disturbance Rejection in a Bearingless Machine with Split-Winding

Rodrigo de Andrade Teixeira [1,†], Werbet Luiz Almeida da Silva [1,†], Adson Emanuel Santos Amaral [2,†], Walter Martins Rodrigues [3,†], Andrés Ortiz Salazar [1,†] and Elmer Rolando Llanos Villarreal [3,*,†]

1   Department of Computer Engineering and Automation, Federal University of Rio Grande do Norte (DCA-UFRN), Natal 59072-970, Brazil
2   School of Science and Technology, University of Rio Grande do Norte (UFRN), Natal 59072-970, Brazil
3   Department of Natural Sciences, Mathematics, and Statistics, Federal Rural University of Semi-Arid (DCME-UFERSA), Mossoró 59625-900, Brazil
*   Correspondence: elmerllanos@ufersa.edu.br
†   These authors contributed equally to this work.

Abstract: In this paper it is proposed the displacement control of a bearingless induction machine (BIM) with split winding and optimized drive structure using Active Disturbance Rejection Control (ADRC). Considering that the BIM is a multivariable, nonlinear, and time-varying system with coupled variables, advanced control techniques can be useful in order to make the system operate efficiently and with good dynamic performance. The ADRC considers the total disturbance, composed of unmodeled dynamics, nonlinearities, uncertainties, and load variations, as an extended state and estimates it in real-time through a state observer. This increases the overall robustness of the control system to disturbances of different natures. The application of the ADRC technique on the radial position control of the BIM used in this work showed that a Linear version of ADRC is not able to compensate for radial load disturbances but this drawback can be solved by the use of a nonlinear observer in the ADRC structure. Besides that, both control versions of the ADRC were able to make stable the naturally unstable radial displacement of the machine's rotor.

Keywords: ADRC control; induction machine; radial position control

1. Introduction

Magnetically suspended induction machines meet a specific industry demand for less noisy motors that can reach higher speeds and do not cause product contamination in situations where the machine directly handles the process. The induction motor is a multivariable, nonlinear system [1] that has a strong coupling between variables. When used in bearingless systems, the degree of control complexity is even greater, especially when placed in situations with shaft load application. In these cases, linear controllers may not achieve a sufficiently fast and stable response for adequate suspension and control of the other system parameters. The emergence of microprocessor devices and power electronics has provided conditions for the application of advanced control theories such as predictive controllers, sliding mode controllers, neural and artificial network-based controllers, Fuzzy controllers, and others [2].

In recent years, the ADRC technique has been used for the control of various types of systems [3–8]. ADRC is a robust control technique that uses state observers in order to estimate in real time the disturbances and uncertainties involved in the controlled process, and from this estimation obtains a good capacity to reject disturbances [9]. ADRC Control is a controller originally based on nonlinear functions, composed of three main blocks: Tracking Differentiator (TD), Extended State Observer (ESO), and the block corresponding to the control law that has received different contributions over the years. The tracking

differentiator provides a smoothed version of the input signal and its derivatives. The extended state observer processes the control signal and the system output to estimate the states variables of the process.

As a fundamental step in the acceptance process of a new control technique in industrial systems, the ADRC is being tested in many different systems. Experimental runs are creating information about the applicability of this control technique, and its potential and limitations are being discovered. Furthermore, the characteristics of the bearingless machine with split-winding with optimized drive structure, such as the natural unstable behavior of radial displacement outputs and complexities of the electrical machine itself makes the process of extending the results obtained by other systems to the BIM complex.

This work investigated the application of ADRC controllers to the position control of a bearingless split-winding induction machine, aiming to understand the limitations of applying this type of controller to the motor-bearing system and to explore the benefits that a technique with active disturbance rejection can bring to radial position control. Keeping the linear structure of the ADRC fixed, this paper analyzed two extended state observer structures. The first structure uses a linear observer and the second structure uses a nonlinear extended state observer, which makes it possible to observe the influence of the addition of nonlinearities on the dynamic performance of the system.

The remainder of the article is structured as follows: Section 2 shows the electrical structure of the BIM with a split-winding and optimized driving system. Section 3 shows the structure of the ADRC controller, the structure of the LADRC controller, and the control structures using linear and nonlinear observer. Section 4 describes the experimental bench used and the control algorithm implemented. Section 5 shows and discusses the experimental results and Section 6 reports the conclusion of the work.

In [10,11] investigates the application of the Active Disturbance Rejection Control (ADRC) technique on the stabilization and control of the rotor radial position of a bearingless induction machine with split winding.

2. Split-Winding Bearingless Motor

The first split-winding bearing motor was proposed by Salazar & Stephan [12]. They built a 4-pole two-phase motor that used the motor's torque coils for radial force generation. In this topology, only one of the phases was responsible for radial position control and both phases were used for torque generation. The two-phase motor proposed by [12] was the starting point for the work of [13], who proposed a three-phase motor in which the coils of each phase were divided into two. In this topology, the three phases were used in the generation of radial force and torque. In [14], the speed vector control of the three-phase motor-mancal was done using neural networks for rotor flux estimation. In this work, the performance of the machine operating with a conventional state estimator and with a neural state estimator was compared. In [15], analyzed the feasibility of using a conventional induction machine as a split-winding bearingless motor. He performed position and current control of the machine, however, he observed that radial position control was not satisfactory for speeds below rated. Ref. [16] studied the replacement of PID controllers for radial position control with controllers based on Fuzzy logic. Noting the strong nonlinear and parameter-varying characteristics of induction motor bearings, he analyzed the contribution of Fuzzy controllers on transient and permanent regime performance. In order to reduce the number of equipment needed for machine control, Ref. [17] optimized the structure of the motor bearing by proposing a new way to connect the coils in the machine stator. In [17] investigated the spatial distribution of the machine's coils and realized that it was possible to generate the radial position control components using only two phases. In this topology, the coils of one of the machine phases are connected directly to the center point of the inverter's DC bus. In this way, only two phases are controlled and the drive structure is optimized.

In this paper, the ADRC control technique is applied with two different structures to the control of a bearingless induction machine, the first structure uses linear estimation

while the second uses nonlinear estimation. The results obtained show the dynamic behavior of the system output and states for the two versions.

Operation Principle

In the bearingless split-winding induction machine, the electric currents in the stator and rotor coils generate magnetic fields that interact with each other. As a result of this interaction, forces arise that act on the rotor, promoting its rotation and radial positioning. In the stator of the three-phase bearing motor, there are three divided groups of windings, where each phase is displaced by 120° relative to the others. With this distribution, it is possible to control the radial positioning of the rotor in all directions from the composition of the radial forces generated. Figure 1 shows the position of the windings relative to the X and Y axes.
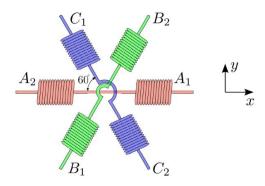

Figure 1. Spatial arrangement of the stator windings of a bearingless induction motor with split winding.

In the optimization proposal by Ref. [17], the coil connection arrangement was modified to the structure shown in Figure 2. This modification reduced the number of control and drive components for the currents in each phase.
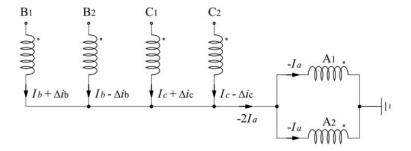

Figure 2. Connection of the coils for two-phase position control.

Considering the currents I_b and I_c are given respectively by:

$$I_b = I_m cos(\omega t - \frac{2\pi}{3})$$
$$I_c = I_m cos(\omega t + \frac{2\pi}{3})$$

(1)

The sum of these currents, for the circuit in Figure 2 results in:

$$I_b + I_c = I_m cos(\omega t)$$

(2)

Since $I_b + I_c = -I_a$, it can be seen that for the modification performed by Ref. [17], the characteristics of the coil currents of phase A have been preserved.

We will illustrate the behavior of the currents per phase in the split-wound three-phase induction machine driven by a 4-arm inverter. Figure 3 shows the waveforms of the currents in each phase for the situation where the rotor is centered on the air gap. When

the rotor is centered, the modulation components are zero, therefore the phase currents have the same modulus $I_a = I_b = I_c$.
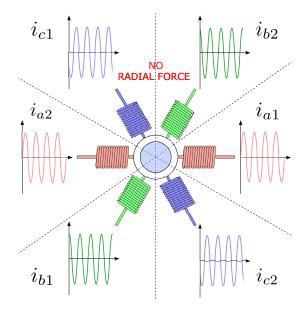
Figure 3. Stator of the bearingless induction motor with split winding.

When unbalance occurs in one of the modulation components or disturbances that tend to move the rotor radially, the phase currents are altered by the control system in order to generate radial forces that bring the rotor back to the center of the stator.

Figure 4 shows the behavior of the currents during radial force generation to the right. To move the rotor shaft in the indicated direction, the control system must increase the currents of coils B_1 and C_2, and reduce the currents of coils B_2 and C_1.
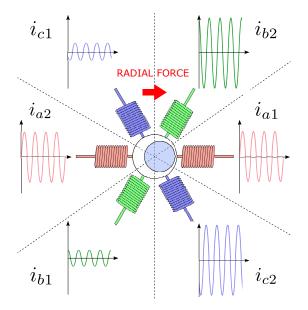
Figure 4. Stator of the bearingless induction motor with split-winding subjected to right-side radial force.

3. ADRC Control

Modern control theory is focused on the time domain and can be applied to systems with multiple inputs and outputs, linear and nonlinear systems, and time-varying and time-invariant systems. One of the difficulties of modern state feedback control systems is that some variables are not accessible by measurement. In this sense, the concept of

a state observer becomes very useful to reconstruct non-measurable state variables from measurable variables. The Active Disturbance Rejection Control technique uses state observers to estimate in real-time the disturbances involved in the controlled process and then uses this information to obtain a good disturbance rejection capability [9].

The structure of an ADRC controller is implemented based on three blocks: a reference generator, controller, and estimator. Figure 5 shows the general idea of a generic process controlled by an ADRC structure. The reference generator block provides a smoothed version of the input signal and its derivatives. The estimator processes the control signal and the system output to estimate the state variables of the process. As will be shown soon in this section, the ADRC structure includes an additional state on the estimator that lump all system uncertainties and disturbances. As the estimator provides a numeric value to the additional state, its effect is removed from the control loop by means of an internal feed-forward loop. This mechanism simplifies the natural plant dynamic from the controller block point of view. This way the controller only needs to deal with an emulated and simpler plant.
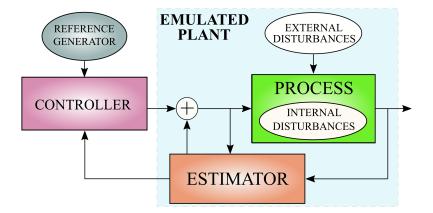

Figure 5. General idea of the ADRC controller.

To provide a mathematical approach to the general idea of an ADRC controller, let us consider a generic second-order process given by:

$$\ddot{y} \quad = \quad -a\dot{y} - by + w + bu \tag{3}$$

where y is the output; u is the input; w represents an external disturbance; a and b are system parameters. By the control systems literature, the parameter b is equivalent to the system input gain. Considering that the numeric value of b is not available, it is possible to consider that $b \approx b_0$ and the difference between the real and the approximated value can be included to the system dynamic in Equation (3) by:

$$\ddot{y} = -a\dot{y} - by + w + (b - b_0)u + b_0 u \tag{4}$$

The term $b - b_0$ is part of the uncertainty in the system model. Consider that all unknown terms of Equation (3) can be grouped and a unique variable is used instead them:

$$\ddot{y} = f + b_0 u \tag{5}$$

This way, $f = -a\dot{y} - by + w + (b - b_0)u$. The variable f is named in the ADRC technique as generalized disturbance and its value is equivalent to the combined effect of dynamic uncertainties, external, internal, and time-varying disturbances, nonlinearities,

and internal parameter variations. Assuming $x_1 = y$ and $x_2 = \dot{x}_1$, the state space form of Equation (5) is given by:

$$
\begin{aligned}
\dot{x}_1 &= x_2 \\
\dot{x}_2 &= f + b_0 u \\
y &= x_1
\end{aligned}
\tag{6}
$$

The key point of the ADRC technique is to use an estimated numeric value of the generalized disturbance f to remove its effect from the dynamics of the controlled process (6) using a simple algebraic operation such as:

$$
u = \frac{u_0 - f}{b_0}
\tag{7}
$$

This operation changes the original dynamic of Equation (6) to a simpler emulated second order dynamic such as:

$$
\begin{aligned}
\dot{x}_1 &= x_2 \\
\dot{x}_2 &= u_0 \\
y &= x_1
\end{aligned}
\tag{8}
$$

The block diagram of the ADRC control of the process represented by Equation (5) is represented in Figure 6, in which the additional state given by the Estimator block is equal to the generalized disturbance variable f.
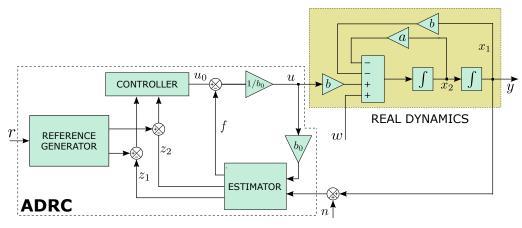

Figure 6. ADRC block diagram of a generic second order plant.

The disturbance rejection mechanism given by the estimation of the general disturbance and the algebraic operation (7) makes the controller see the real dynamics as a more simple plant. This way, the block diagram of Figure 6 is virtually reduced to the diagram of Figure 7.
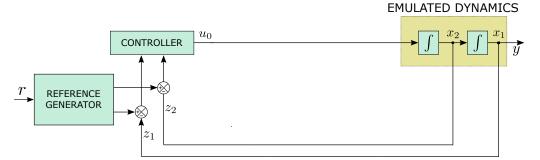

Figure 7. Equivalent block diagram.

The generalized disturbance is capable of encompassing a wide range of uncertainties and effects, such as: external and time-varying disturbances, unmodeled internal dynamics, nonlinearities, and internal parameter variations. ADRC groups these uncertainties and effects and uses this information to remove the effects of this information from the process control.

In Gao [18] a linear structure for ADRC applied to second-order systems was proposed, in which the controller and estimator (called the Linear Extended State Observer—LESO) are fully linear functions. Furthermore, this structure does not use the reference generator block. The block diagram in Figure 8 shows the application of linear ADRC to a second-order G_p system.
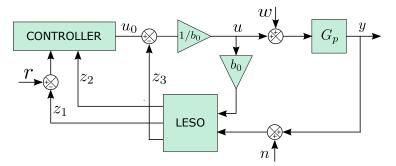

Figure 8. LADRC block diagram.

The output y is controlled by a LADRC from the application of input r. The states estimated by the linear extended state observer (LESO) are given by z_1, z_2, and z_3. The estimated state z_3 is equal to the generalized disturbance f of the Equation (5). The parameter b_0 is a tuning parameter. The external disturbances are represented by: w (input disturbance) and n (measurement noise).

Using the linear ADRC structure proposed in [18] this paper analyzed the application of two extended state observer structures. The first structure uses a linear observer with a saturator at the output, as shown in Figure 9a.
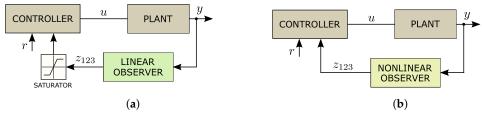

Figure 9. Block diagrams of the implemented controllers. (**a**) Linear ADRC. (**b**) Nonlinear ADRC.

The saturator block in the LADRC structure was necessary because the effect of peak phenomenon [19] impossible the stabilization of the radial displacement outputs due to the synchronous disturbances that are present in this type of system, as described in the work [20]. The second structure uses a nonlinear extended state observer as shown in Figure 9b. This structure makes it possible to observe the influence of adding the nonlinearities on the dynamic performance of the system.

4. Description of the System

4.1. System Overview

Figure 10 provides an overview of the bench. The equipment has been grouped into the following blocks: monitoring and control, power supply circuit, and bearingless machine.
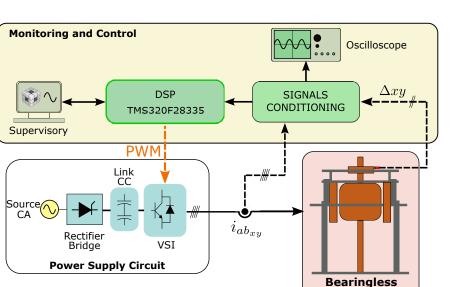
Figure 10. Overview of the components of the experimental bench.

The bearingless machine block consists of the bearingless electric induction machine on which the tests were performed. The power supply circuit block comprises the entire infrastructure of electronic components and equipment responsible for providing the power supply at the appropriate levels to control the machine variables. This is achieved by a three-phase Voltage Source Inverter (VSI). The monitoring and control block consists of the electronic circuits, Digital Signal processor (DSP), and monitoring devices that were necessary to implement the system's control and supervision routines. The variable i_{abxy} represents the four-phase electrical connections that allow the drive block to supply controlled electrical currents to the bearing motor. Figure 10 also indicates the reading of these i_{abxy} currents performed by the monitoring and control block. The variable Δ_{xy} represents the signals corresponding to the radial positions of the *x* and *y* axes of the bearing motor read by the monitoring and control block. Finally, the orange arrow named PWM indicates the signals sent by the monitoring and control block to the drive block.

Figure 11 shows a real image of the experimental bench. This structure is located in the Laboratory in the Computer and Automation Engineering Department at UFRN.
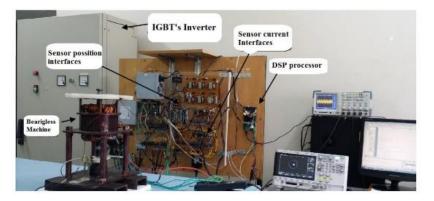

Figure 11. Experimental bench.

4.2. Split-Winding Bearingless Machine

The prototype used works vertically with the goal of simplifying radial position control. The machine's rotor is supported in the axial position by a mechanical bearing that is also responsible for fixing the machine's lower end. Figure 12 shows the prototype.
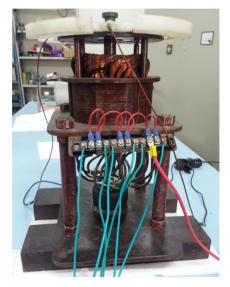
Figure 12. Split-winding bearing machine prototype.

The electrical data of the machine is detailed in Table 1.

Table 1. Machine parameters.

Parameters	Values
Frequency	60 Hz
Poles number	4
Supply voltage	220/380 V
Current	3.02/1.75 A
No-load current	1.9 A
No-load power	160 W
Stator resistance per phase	0.63 Ohm

4.3. DSP TMS320F28335

The *DSP TMS*320*F*28335 is a digital signal controller that has the characteristics of a conventional processor because it contains in its structure circuits capable of executing programs stored in memories and also has additional circuits for digital signal processing, which includes hardware with special architecture and instructions for mathematical calculations and are able to perform real-time operations. In addition, the *TMS*320*F*28335 has in its structure memory and programmable input and output components, which also makes the *TMS*320*F*28335 a microcontroller.

4.4. Control Algorithm Implementation

The block diagram in Figure 13 shows the blocks needed for the practical experiments with the system. With the exception of the inverter block, all other blocks were implemented in *C* language in the *DSP* programming interface.

The general idea of the control algorithm is the existence of two cascaded control loops: the current control loop, with fast dynamic response and with the objective of making the currents in the controlled phases follow the specified reference; and the position control loop, which has slower dynamics than the current control loop and operates in a more external way, generating the references for the current control loop. The position control loop aims to maintain the radial position at the reference values Y_{ref} and X_{ref}, for this, the position control signals are added to the magnetization currents I_m to generate the necessary currents for the positioning of the rotor radial.
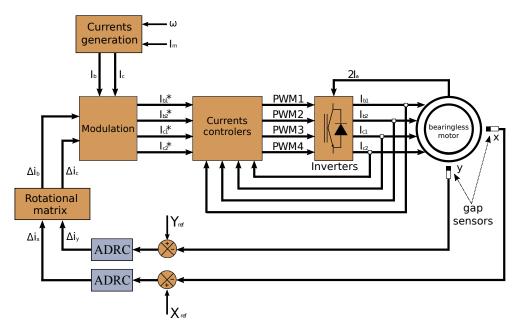
Figure 13. Control system diagram.

The bias current block is responsible for generating via software the magnetizing currents of the machine. This block implements Equations (1) and its arguments are the angular velocity and the peak value of the magnetizing currents. In the control algorithm, there are two ADRC blocks, one for each radial positioning axis of the machine. These blocks implement all the blocks required in the structure of the ADRC technique. These blocks receive the error calculated from subtracting the radial positions of the rotor by its references Y_{ref} and X_{ref} and perform the necessary operations to generate the correction signal $\Delta_i y$ and $\Delta_i x$. The rotational transformation block converts the control signals calculated in the x–y positioning referential to b–c corresponding to the spatial alignment of the controlled motor-manifold coils. The function of the modulation block is to perform the composition of the rotation currents I_b and I_c with the control signals $\Delta_i b$ and Δ_{ic} and thus generate the references I_{b1}^*, I_{b2}^*, I_{c1}^* and I_{c2}^*. Finally, the current control block implements four digital PI controllers, which monitor the machine currents and generate the PWM control signals for driving the inverters.

5. Experimental Results and Discussion

Two versions of ADRC controllers have been implemented in the DSP TMS320F28335. The first one used the linear form proposed by Gao in [18] for the extended observer and the PD controller. The other version used fal-type nonlinearities in the observer structure. The results in three dimensions for the two implemented controllers can be seen in Figure 14.

Figure 14a shows the behavior of positions X and Y in steady state for the first version of the controller. A mean error of -1.17% with a standard deviation of 0.03 mm was obtained for the X axis. As for the Y-axis, an average error of 0.76% with a standard deviation of 0.05 mm was obtained. Figure 14b shows the behavior of the X and Y positions in a steady state for the version with nonlinearities. The mean error for the X-axis was -0.09% with a standard deviation of 0.07 mm. For the Y axis, the mean error was -0.05% with a standard deviation also of 0.05 mm. The results indicate the effect of adding non-linearity on the observer's structure. It was possible to improve the regime error with the non-linear versions, but the variation around the reference became more evident, indicating an increase in the aggressiveness of the controller response.
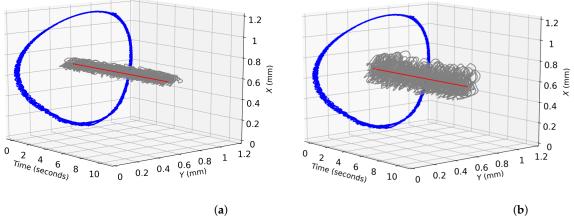
(**a**) (**b**)

Figure 14. Steady state response of radial position control for the linear and nonlinear controllers in 3D. (**a**) Linear ADRC. (**b**) Nonlinear ADRC.

Figure 15a,b shows the behavior of the radial position signals when there are step-type reference variations in the X-axis only, keeping the Y- axis reference fixed, and Figure 15c,d when step-type variations occur in Y, keeping the X-axis reference is fixed.

The results in Figure 15 show that step variations in one of the axes do not result in a significant influence on the dynamic behavior of the opposite axis. The same test was performed to the controller with a nonlinear observer; the results are shown in Figure 16. The results obtained indicate that there is a decoupling in the dynamic behavior of the radial position between the two axes.
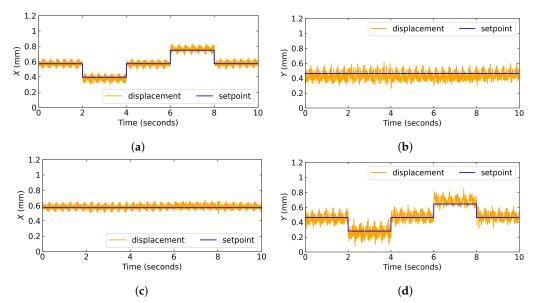

(**a**) (**b**)

(**c**) (**d**)

Figure 15. Response of radial position control under step setpoint changes for Linear ADRC. (**a**) X-axis behavior with step setpoint changes applied. (**b**) Y-axis behavior with step setpoint changes applied to X-axis. (**c**) X-axis behavior with step setpoint changes applied to Y-axis. (**d**) Y-axis behavior with step setpoint changes applied.

The addition of a radial load to the machine shaft in operation is an important analysis since this load is seen by the position controllers as an external disturbance in the form of a step. Therefore, it is a simple way to impose a perturbation and analyze the robustness of the controller in situations such as this. For this analysis, an apparatus that allowed the addition of a radial load aligned with the X-axis was used. Figure 17 illustrates how the device was used to add the radial disturbance.
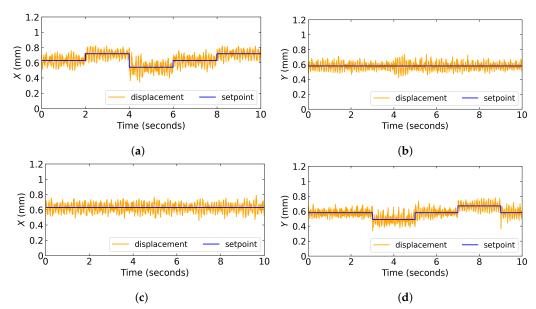
Figure 16. Response of radial position control under step setpoint changes for Nonlinear ADRC. (**a**) *X*-axis behavior with step setpoint changes applied. (**b**) *Y*-axis behavior with step setpoint changes applied to *X*-axis. (**c**) *X*-axis behavior with step setpoint changes applied to *Y*-axis. (**d**) *Y*-axis behavior with step setpoint changes applied.
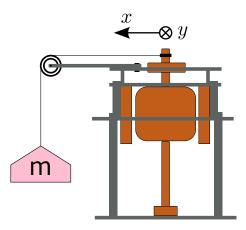

Figure 17. Illustrative image of the machine subjected to load addition.

For each controller, the z_1, z_2, and z_3 states of the *X* and *Y* axes were collected in a time interval that allowed detecting the exact instant of addition of the radial load to the machine axis. Figures 18 and 19 show the behavior of the states of the *X* and *Y* axes for the two implemented controllers. In each graph, a green dashed vertical line was inserted to indicate the instant the application of 150 g of radial load aligned to the *X*-axis. This load was inserted in such a way that the radial load tends to move the radial position in the positive direction of the axis. Figure 18a,b show the state behavior of the linear controller. Visually, it is possible to state that there was a certain degree of rejection of the radial disturbance, but it is evident that the regime error of the *X*-axis increased after the moment of application of the load. The *Y*-axis remained stable. It is not possible to perceive variations in the z_3 state on the scale used because the linear controller was implemented with saturators at the observers' output in order to avoid the Peak phenomenon.
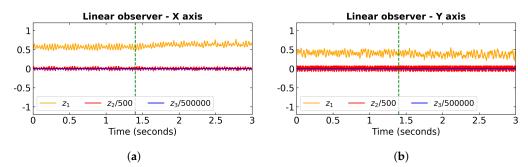
Figure 18. Estimated states behavior for linear ADRC under radial load application. (**a**) Linear ADRC—*X*-axis states. (**b**) Linear ADRC—*Y*-axis states.
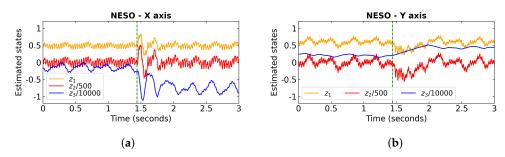

Figure 19. Estimated states behavior for nonlinear ADRC under radial load application. (**a**) Nonlinear ADRC—*X*-axis states. (**b**) Nonlinear ADRC—*Y*-axis states.

Through the analysis of the z_1 states of Figure 19a,b. it is possible to conclude that the ADRC controller with NESO was less influenced by the application of the radial load in the steady state since qualitatively the response was very similar for the intervals before and after the addition of the disturbance. The behavior of the states indicated an aggressive reaction of the controller in the transient regime, resulting in high values of z_2 during this region of the collection. The change in the mean value observed for the z_3 state indicates that this variable was able to identify the addition of the external disturbance. The good rejection of the observed perturbation may be a result of this. Quantitatively, the results of Figures 18 and 19 can be summarized according to Table 2. Table 2 shows the average values in a steady state of the observed states.

Table 2. Mean values of the states estimated by the linear and nonlinear ESO before and after the radial load application.

Controller	State z_1		State z_2		State z_3	
Load Application	Before	After	Before	After	Before	After
Linear ESO	0.57	0.64	−0.32	−0.33	1.64	−7
Nonlinear ESO	0.48	0.48	−1.34	−2.6	−1522	−7909

The value of the z_1 state for the linear controller indicates that there was a displacement of the mean value of the output after applying the load. This is a limitation of the linear observer as its states the need to read limited amplitude to avoid peak phenomenon and guarantee stability. As indicated by the value of z_3 after applying the load, it was blocked in the imposed saturation. The saturation of state outputs impairs the ability to reject disturbances. The mean value of the z_1 state of the non-linear indicates that it was able to reject the load addition. Furthermore, the significant change in the value of z_3 shows that it was able to identify the disturbance.

The value of z_3 in Table 2 becomes more negative after adding the load because the control loop error is given by:

$$Error = pos - ref \tag{9}$$

that is, when the radial position is displaced from the reference value in the sense of increasing the error value, the control signal must increase in order to restore the equilibrium position close to the reference. Knowing that the control signal is calculated by:

$$u = \frac{u_0 - z_3}{b_0} \tag{10}$$

it means that the more negative the value of z_3, the greater the values of the control signals and the greater the control effort in the sense of rejecting the action of the disturbance in the system output. The more positive the displacement value is in relation to the reference, the greater the control signal must be.

Finally, to analyze the relationship between the value of z_3 and the intensity of the radial disturbance applied to the motor shaft and also to verify to what extent the system could reject the radial load, masses of 32 g were added one by one in the application support of the load. This test was performed with the NESO-based controller only. In the first step, the radial load support was aligned on the X-axis and then on the Y-axis. For each added mass, the regime errors of the X and Y positions were calculated and the z_3 states were collected. The results are shown in Figures 20 and 21. Figure 20 shows the results for the radial load bearing aligned with the X-axis.
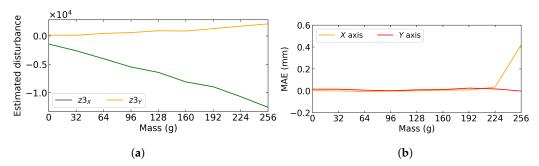
Figure 20. Generalized disturbance estimation and mean steady state error for X and Y axes to different values of radial load aligned with the X-axis. (**a**) Generalized disturbance estimation (z_3). (**b**) Mean absolute error for X and Y axes.
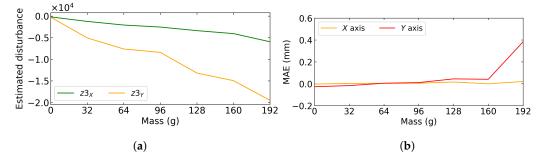
Figure 21. Generalized disturbance estimation and mean steady state error for X and Y axes to different values of radial load aligned with the Y-axis. (**a**) Generalized disturbance estimation (z_3). (**b**) Mean absolute error for X and Y axes.

Figure 20b shows that the regime error remained close to zero for loads of up to 224 g. When the radial load increased to 256 g, the position control in the X-axis became unstable but remained stable on the Y-axis. Figure 20a shows the estimation of generalized disturbances for the X and Y axes increase in load and the z_3 state of the X-axis. This variable becomes more negative as the load increases, as expected. Figure 20a also shows that the load added in the X direction also influenced the z_3 state of the Y axis. This indicates that the load support was not perfectly aligned with the desired axis, or that the X and Y sensors could not have been perfectly spaced 90 degrees apart.

Figure 21 shows the analysis of radial load disturbance for the radial load added in the positive direction of Y. The Y axis showed a lower radial disturbance rejection capacity since it only managed to keep the regime error close to zero up to 160 g of load. The Y-axis control became unstable for the 192-g load, while the X-axis remained stable for all analyzed loads. Figure 21a indicates that there is also an approximately linear relationship between the value of z_3 and the value of the added charge. Likewise, there was a smaller scale detection of radial disturbance by the z_3 state of the X-axis. In this test, the influence on the cross-axis was greater. The results of the load curve for both axes showed that there is a linear relationship between the perturbation and the z_3 state. This relationship is fundamental to the success of the strategy and indicates that the extended state observers are capable of detecting external disturbances without the need for physical sensors installed in the process.

6. Conclusions

This paper examined the ADRC active disturbance rejection technique applied to a bearingless induction machine. Two structures were employed in the laboratory testing for the extended state estimator, one linear and the other nonlinear. For both versions, the step reference variation results exhibit a satisfactory level of dynamic decoupling between the radial displacements in the X and Y axes. The test with load imposition showed that both observers were able to detect the generalized disturbance, however, only the nonlinear observer was able to maintain the same average system output value before and after load application. The results obtained show the success of the ADRC technique in the active estimation and rejection of disturbances in the radial positioning process of a split rotor bearingless machine. The results also show the higher active rejection capability of the technique applied with a nonlinear observer since with this type of observer disturbances of this nature are estimated and compensated.

Author Contributions: R.d.A.T., W.L.A.d.S and A.O.S. conceived and designed the study; R.d.A.T., A.E.S.A. and W.L.A.d.S., methodology; R.d.A.T., A.E.S.A. and W.L.A.d.S. performed the simulations and experiments; E.R.L.V., W.M.R. and A.O.S. reviewed the manuscript and provided valuable suggestions; E.R.L.V., R.d.A.T., W.L.A.d.S. and W.M.R. wrote the paper; supervision, A.O.S. and W.M.R. All authors have read and agreed to the published version of the manuscript.

Conflicts of Interest: The authors declare no conflicts of interest.

Abbreviations

The following abbreviations are used in this manuscript:

BIM	Bearingless Induction Machine
ADRC	Active Disturbance Rejection Control
LADRC	Linear Active Disturbance Rejection Control
ESO	Extended State Observer
LESO	Linear Extended State Observer
NESO	Nonlinear Extended State Observer
TD	Tracking Differentiator
DSP	Digital Signal Processing
PID	Proportional-Integral-Derivative
PD	Proportional-Derivative
PI	Proportional-Integral
PWM	Pulse Width Modulation
DC	Direct Current
VSI	Voltage Source Inverter

References

1. Yang, Z.; Jia, J.; Sun, X.; Xu, T. An enhanced linear adrc strategy for a bearingless induction motor. *IEEE Trans. Transp. Electrif.* **2021**, *8*, 1255–1266. [CrossRef]
2. Yang, Z.; Ji, J.; Sun, X.; Zhu, H.; Zhao, Q.Q. Active Disturbance Rejection Control for Bearingless Induction Motor Based on Hyperbolic Tangent Tracking Differentiator. *IEEE J. Emerg. Sel. Top. Power Electron.* **2020**, *8*, 2623–2633. [CrossRef]
3. Li, J.; Zhang, L.; Li, S.; Mao, Q.; Mao, Y. Active Disturbance Rejection Control for Piezoelectric Smart Structures: A Review. *Machines* **2023**, *11*, 174. [CrossRef]
4. Heidary, J.; Gheisarnejad, M.; Khooban, M.H. Stability Enhancement and Energy Management of AC-DC Microgrid based on Active Disturbance Rejection Control. *Electr. Power Syst. Res.* **2023**, *217*, 109105. [CrossRef]
5. Huang, C.; Zhao, H. Error-Based Active Disturbance Rejection Control for Wind Turbine Output Power Regulation. *IEEE Trans. Sustain. Energy* **2023**, *1*, 1–10. [CrossRef]
6. Zhou, Z.; Li, X.; Tuo, W.; Wang, F. Design of active disturbance rejection control with noise observer for an optical reference unit. *Control Eng. Pract.* **2023**, *132*, 105427. [CrossRef]
7. Shao, X.; Fan, Y.; Shao, J.; Sun, G. Improved active disturbance rejection control with the optimization algorithm for the leg joint control of a hydraulic quadruped robot. *Meas. Control* **2023**, *1*. [CrossRef]
8. Li, J.; Liu, J.; Huangfu, S.; Guoyan Cao, G.; Yu, D. Leader-follower formation of light-weight UAVs with novel active disturbance rejection control. *Appl. Math. Model.* **2023**, *117*, 577–591. [CrossRef]
9. Zhu, L.; Zhang, G.; Jing, R.; Bi, G.; Xiang, R.; Wang, G.; Xu, D. Nonlinear active disturbance rejection control strategy for permanent magnet synchronous motor drives. *IEEE Trans. Energy Convers.* **2022**, *37*, 2119–2129. [CrossRef]
10. Silva, W.L.A.; Salazar, A.O.; Cabral Neto, R.J.N.; Villarreal, E.R.L. Radial Position Control of a Bearingless Machine with Active Disturbance Rejection Control. In *2020 IEEE XXVII International Conference on Electronics*; Electrical Engineering and Computing (INTERCON): Lima, Perú, 2020; pp. 1–5.
11. Silva, W.L.A.; Salazar, A.O.; Vieira, P.V.F.; Jácome, M.C.; Villarreal, E.R.L. Radial Position Control of a Bearingless Machine with Active Disturbance Rejection Control Fuzzy an approach. In Proceedings of the 2021 IEEE International Conference on Automation/XXIV Congress of the Chilean Association of Automatic Control (ICA-ACCA), Online, 22–26 March 2021; pp. 1–5.
12. Salazar, A.O.; Stephan, R.M. A bearingless method for induction machines. *IEEE Trans. Magn.* **1993**, *29*, 2965–2967. [CrossRef]
13. Ferreira, J.M.S.; Salazar, A.O. Máquina de Indução Sem Mancais: Modelo e Acionamento. *Eletrônica de Potência* **2007**, *12*, 2509–2521.
14. De Paiva, J.A.; Salazar, A.O.; Maitelli, A.L. Review of Control Strategies and Model Estimation Techiniques Applied to Bearingless Induction Machine with Divided Winding. In Proceedings of the 1st Brazilian Workshop on Magnetic Bearings, Rio de Janeiro, Brazil, 25–26 October 2013; Volume 1, pp. 1–6.
15. Victor, V.F.; Quintaes, F.O.; Lopes, J.S.B.; Santos Junior, L.D.; Lock, A.S.; Salazar, A.O. Analysis and Study of a Bearingless AC Motor Type Divided Winding, Based on a Conventional Squirrel Cage Induction Motor. *IEEE Trans. Magn.* **2012**, *48*, 3571–3574. [CrossRef]
16. Nunes, E.A.D.F.; Salazar, A.O.; Villarreal, E.R.L.; Souza, F.E.C.; Dos Santos Júnior, L.P.; Lopes, J.S.B.; Luque, J.C.C. Proposal of a fuzzy controller for radial position in a bearingless induction motor. *IEEE Access* **2019**, *7*, 114808–114816. [CrossRef]
17. Carvalho Souza, F.E.; Silva, W.; Ortiz Salazar, A.; Paiva, J.; Moura, D.; Villarreal, E.R.L. A Novel Driving Scheme for Three-Phase Bearingless Induction Machine with Split Winding. *Energies* **2021**, *14*, 4930. [CrossRef]
18. Gao, Z. Scaling and bandwidth-parameterization based controller tuning. In Proceedings of the 2003 American Control Conference, Denver, CO, USA, 4–6 June 2003; Volume 6, pp. 4989–4996.
19. Maopeng, R.; Li, J.; Xie, L. A new extended state observer for uncertain nonlinear systems. *Automatica* **2021**, *131*, 109772.
20. Mota, A.I.P.; Silva, W.L.A.; Souza, F.E.C.; Salazar, A.O. Synchronous disturbance suppression in bearingless machines with active disturbance rejection controller. In Proceedings of the 2021 Brazilian Power Electronics Conference (COBEP), João Pessoa, PB, Brazil, 7–10 November 2021; pp. 1–5.